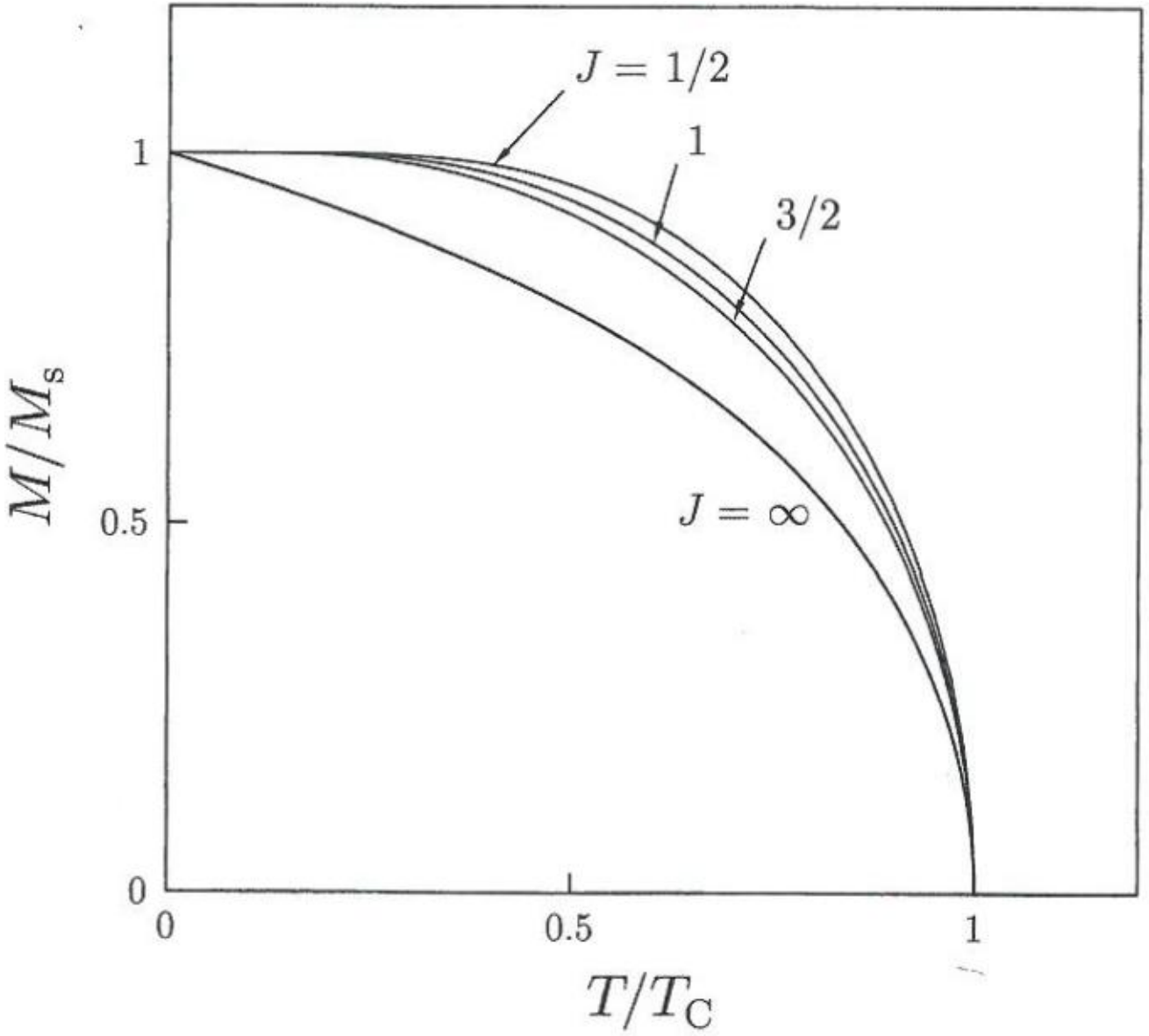

Fig. 5.3 The mean-field magnetization as a function of temperature, deduced for different values of J.

Susceptibility of an antiferromagnet

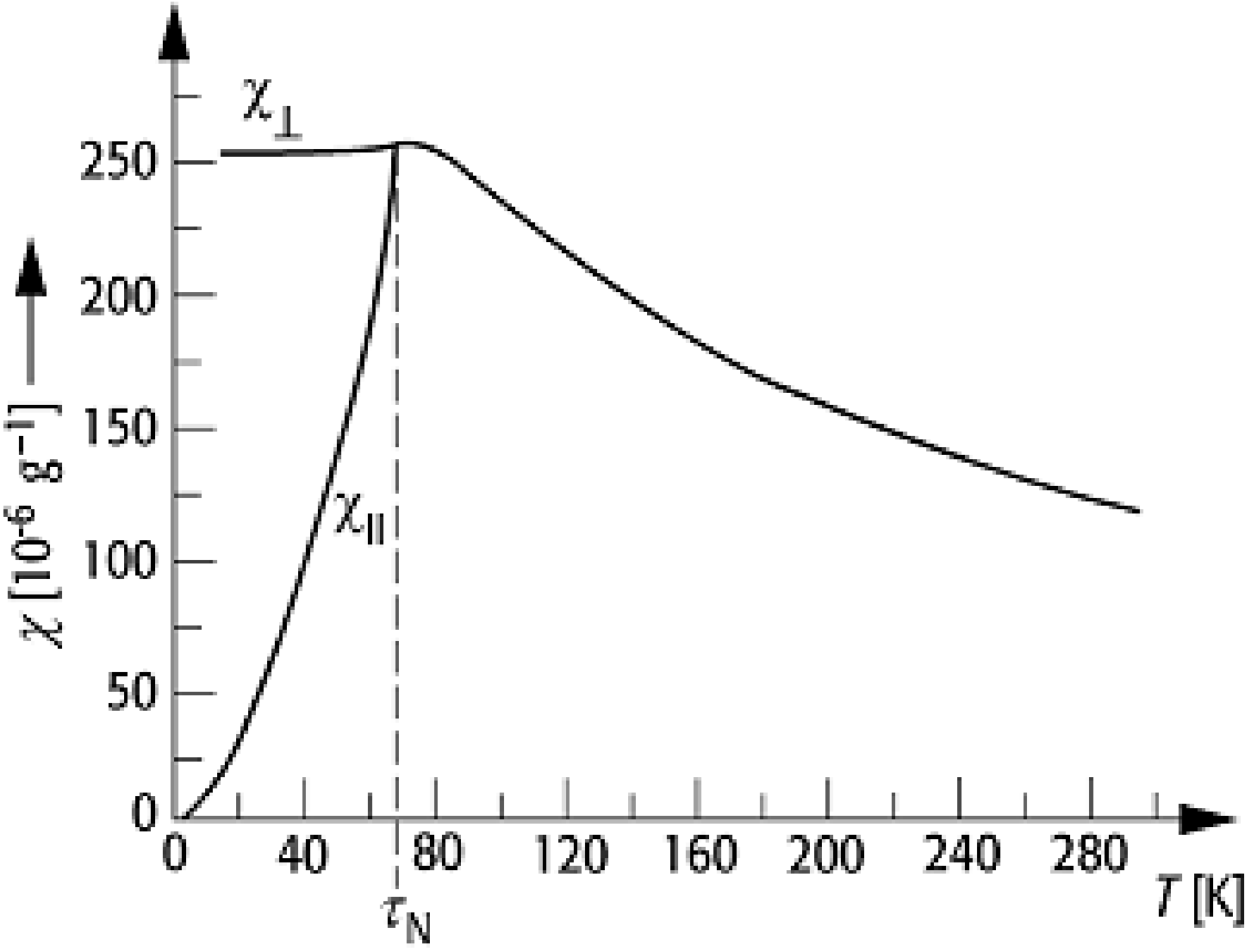

χ(T) – example: spin ladder

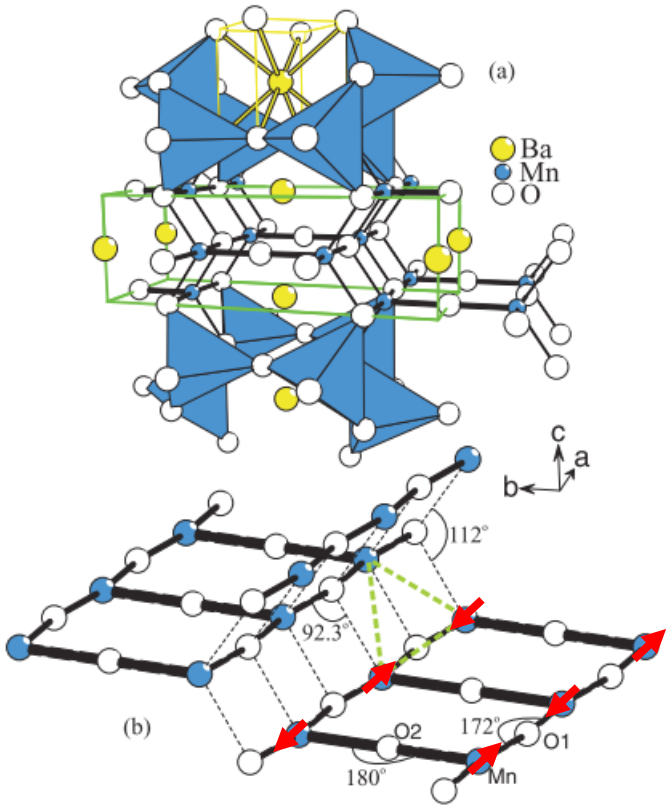

FIG. 1. (Color online) (a) Room-temperature structure of $BaMn_2O_3$. The open balls at the corners of the Mn-containing polyhedra are oxygen atoms; the closed large and small balls represent Mn and Ba ions, respectively. In addition, the unit cell is displayed by lines. (b) A selected part of the structure showing the Mn-O substructure with Mn–O–Mn bond angles. The thick dashed lines indicate the geometrical frustration, as discussed in the text.

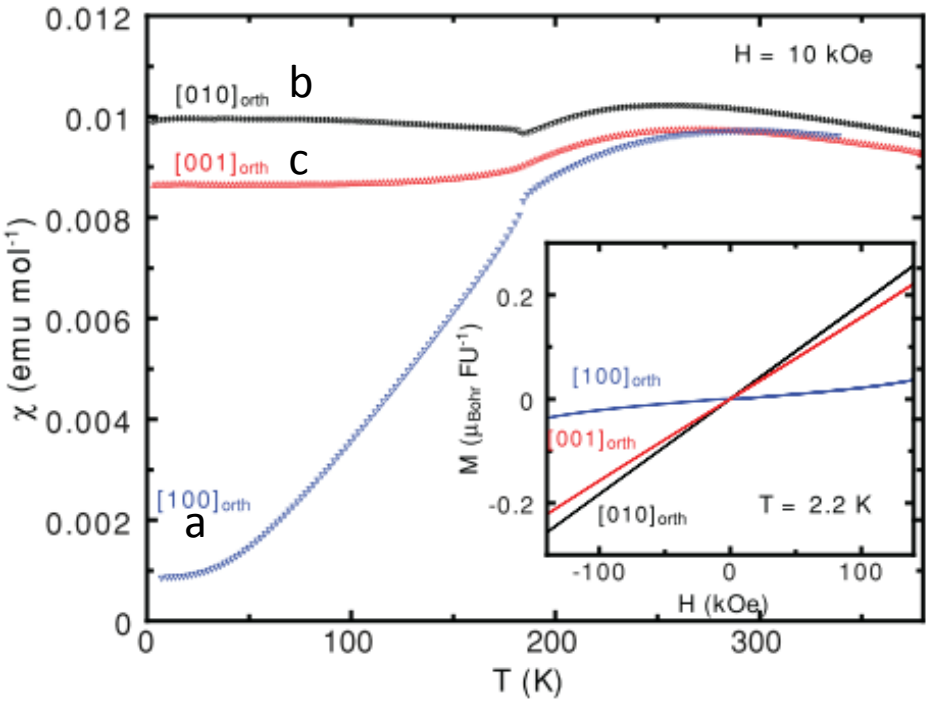

FIG. 2. (Color online) Magnetic susceptibility as a function of temperature measured in magnetic fields of 1 T applied along all three orthorhombic crystallographic directions of $BaMn_2O_3$. The inset displays magnetization curves measured at 2.2 K as a function of the magnetic field up to 14 T applied along the orthorhombic axes.

Magnetic cicular dichroism

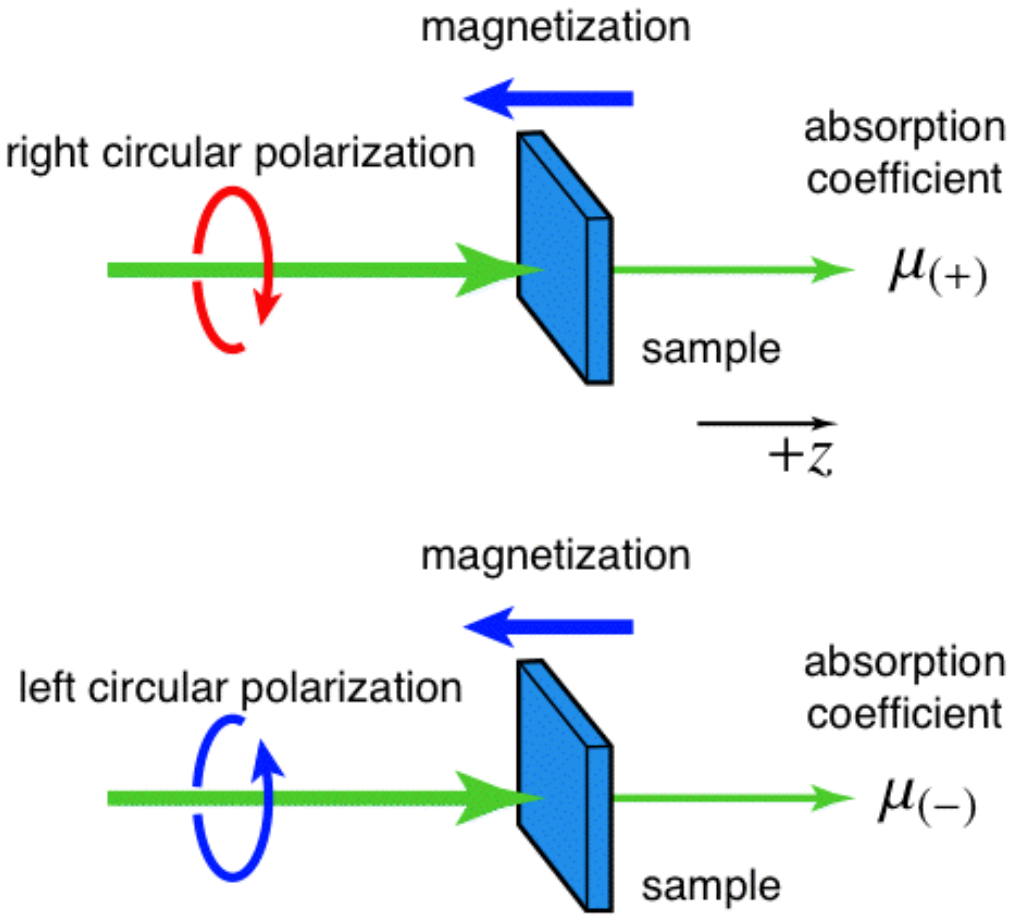

X-ray magnetic circular dichroism (XMCD)

$$\Delta\mu = \mu_{(+)} - \mu_{(-)}$$

XMCD-example

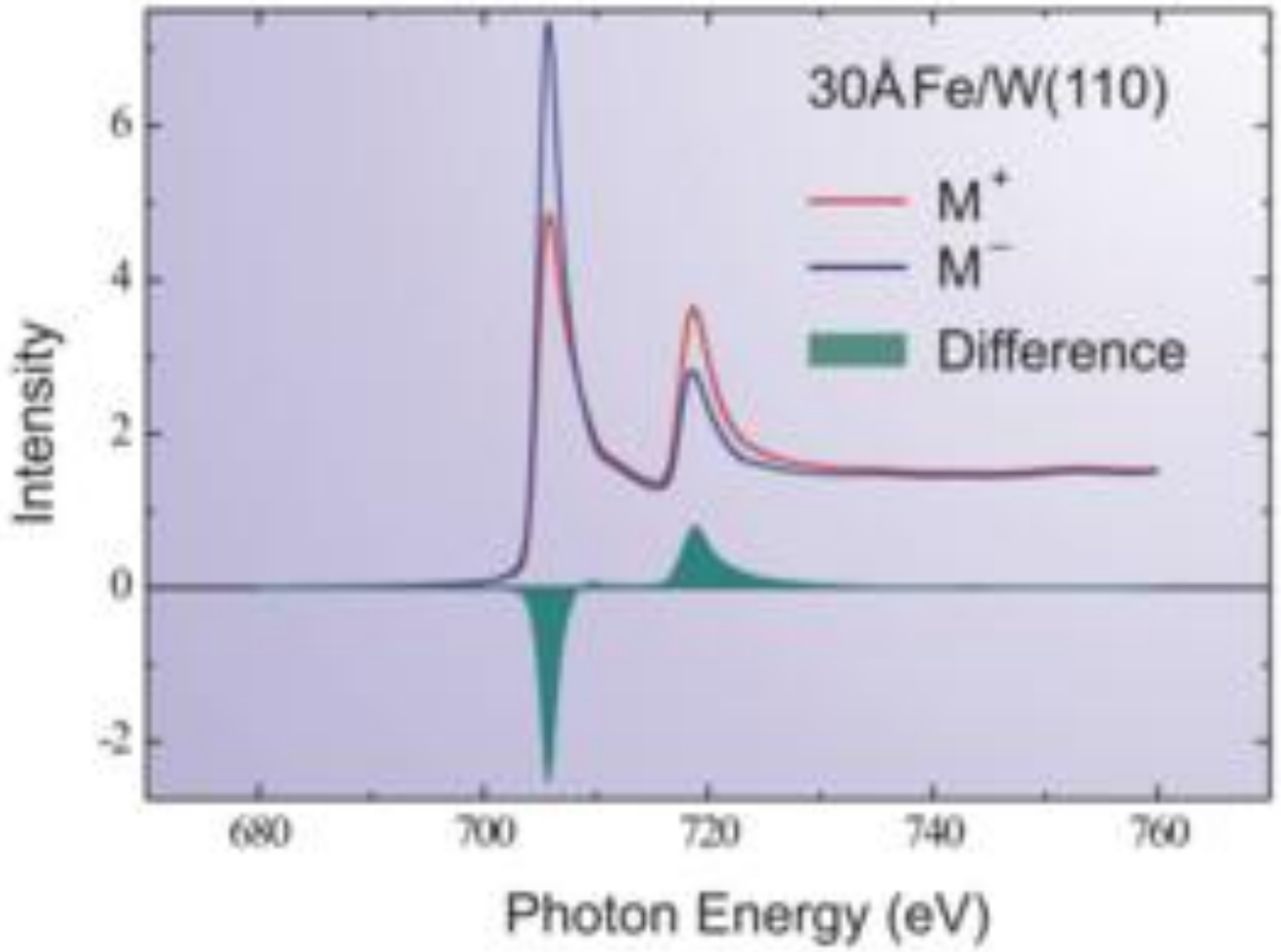

Mott detector

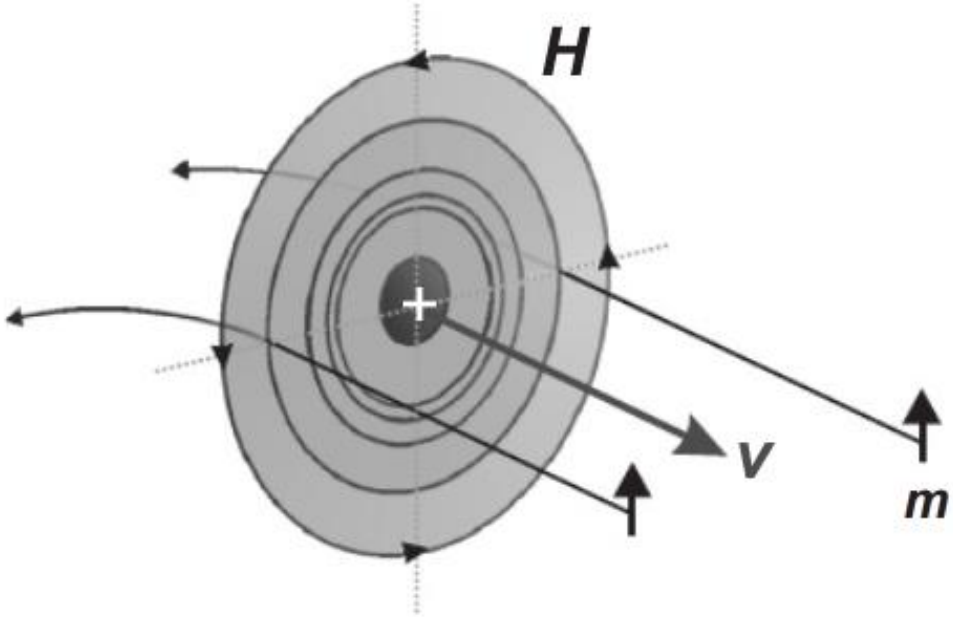

Fig. 3.10. Illustration how spin-orbit coupling in elastic Coulomb scattering can spatially separate the two spin states: The electron with its magnetic moment up is incident on an atom whose projection perpendicular to the incidence direction is shown. In the rest system of the electron, the positive charge of the atomic nucleus moves toward it with a velocity $\boldsymbol{v}$. This is equivalent to an electric current with circular magnetic field lines as shown. The force $\boldsymbol{F}$ on the magnetic moment of the electron is directed toward increasing field when the moment is parallel to the field (*right*), but toward decreasing field when it is antiparallel (*left*). If $\boldsymbol{m}$ and $\boldsymbol{H}$ are perpendicular the force is zero. In this way, the magnetic moment of the electron experiences a force toward the left side when it is aligned upward no matter on which side of the atom it passes. In contrast, electrons with magnetic moment "down" are preferentially scattered to the right in our figure

Mott detector

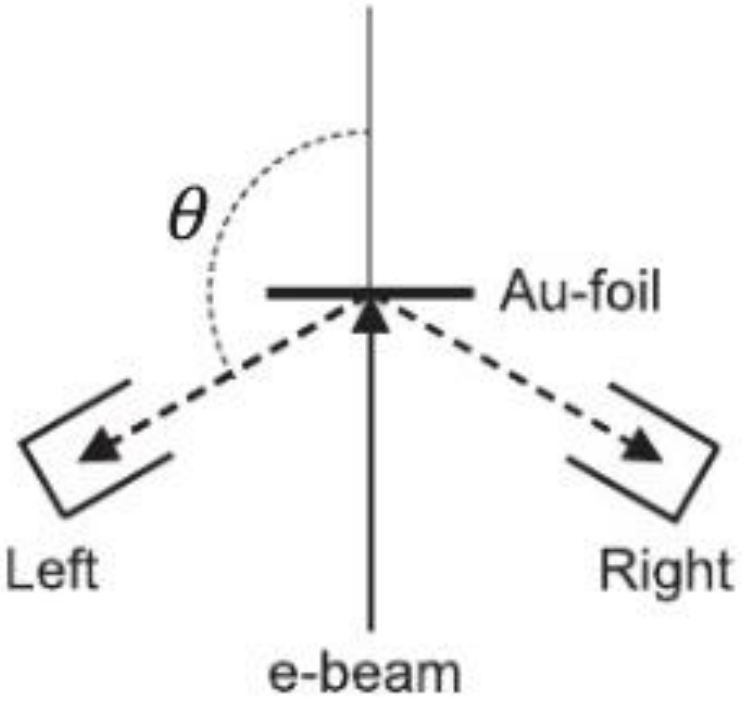

Fig. 3.11. Experimental setup to measure the scattering asymmetry A caused by the spin polarization of an electron beam. The electrons elastically scattered into the scattering angle θ to the right and to the left are measured. If the spins of the electrons in the incident beam are polarized perpendicular to the scattering plane, a scattering asymmetry occurs which is proportional to the degree of spin polarization $P_\perp$.

Spin-resolved ARPES

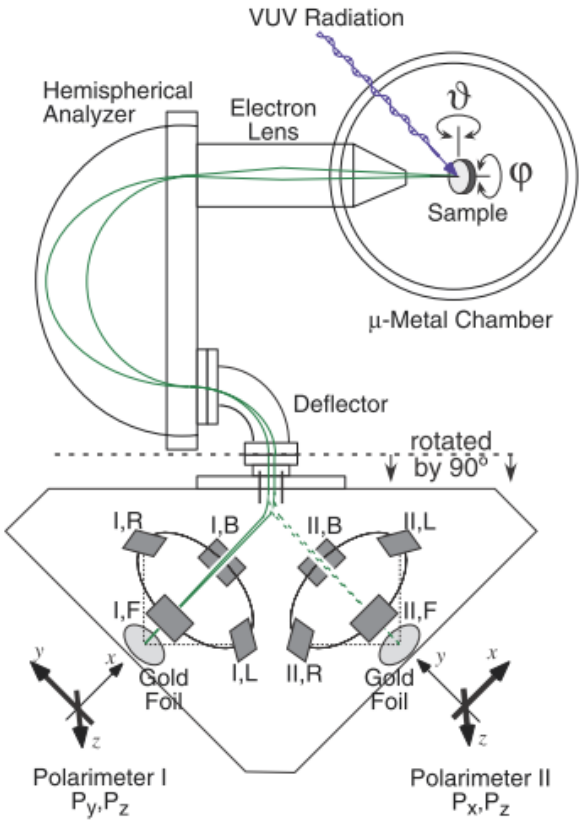

Fig. 5. Schematic view of the three-dimensional polarimeter [7]. Electrons that are photoemitted from a sample by ultraviolet radiation are energy and angle selected by an electrostatic analyzer and detected in two orthogonal Mott polarimeters (named polarimeter I and II). In an electrostatic beam deflection system the spin direction is conserved and polarimeter I measures the polarization components P_y and P_z, while polarimeter II measures P_x and P_z. The beam is switched between the two in order to allow quasi-simultaneous data collection. In the figure, the polarimeter system is shown rotated by 90° for graphical clarity, i.e. in reality the z axis is directed straight to the left and parallel to the electron lens of the spectrometer

SR-ARPES: example

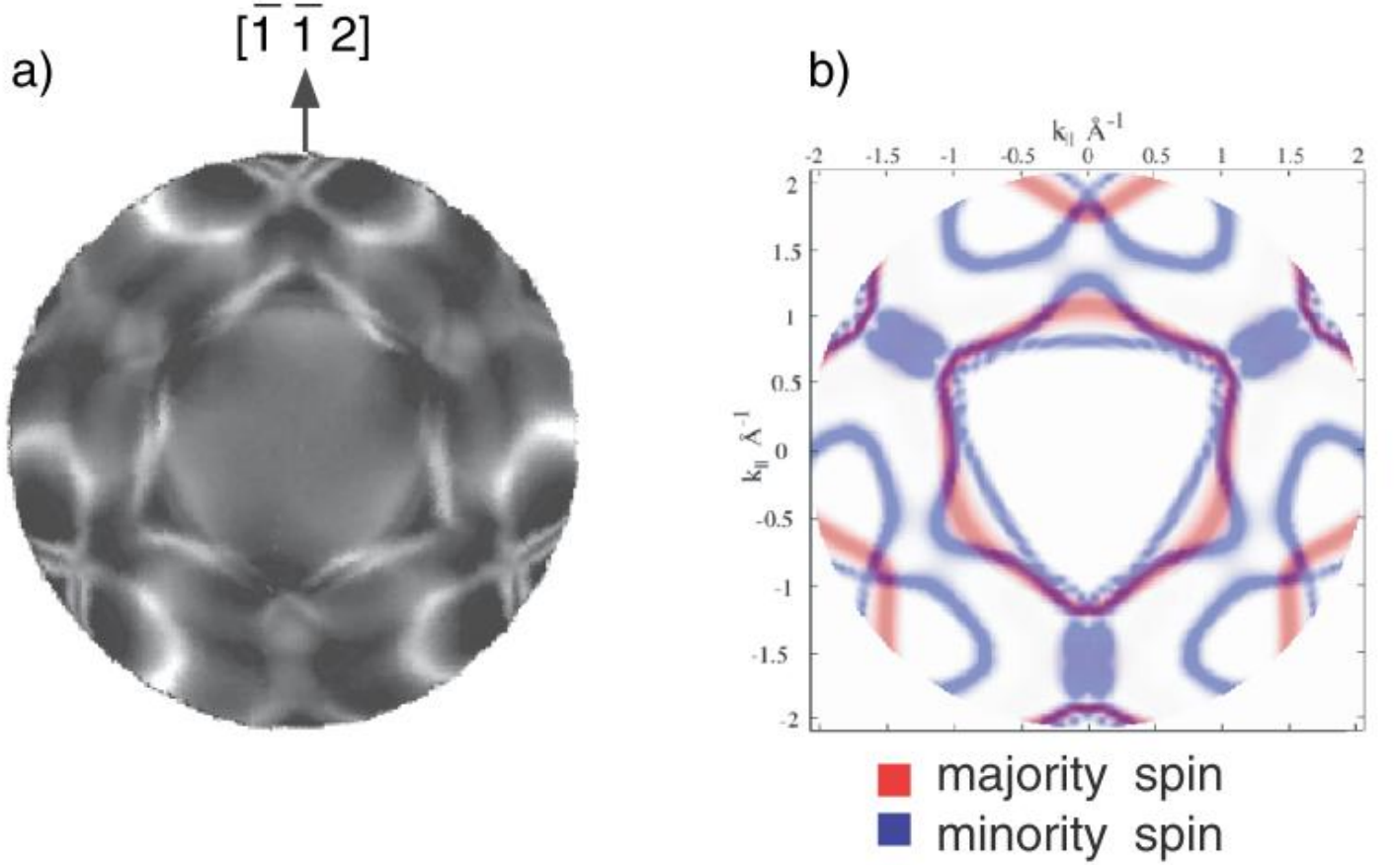

Fig. 2. (**a**) He Iα excited Fermi surface map ($h\nu = 21.21$ eV) from Ni(111). A $\boldsymbol{k}_{\parallel}$ projection of the raw data is presented in a linear grey scale, with highest intensities in white, lowest in black. In (**b**) the corresponding spin-polarized band structure calculation is displayed, showing Fermi level crossings at the same $\boldsymbol{k}_{\parallel}$ locations as in the measurement (a). Majority spin bands are shown in red, minority spin bands in grey (From [10], with improved experimental data by W. Auwärter)

NMR experiment

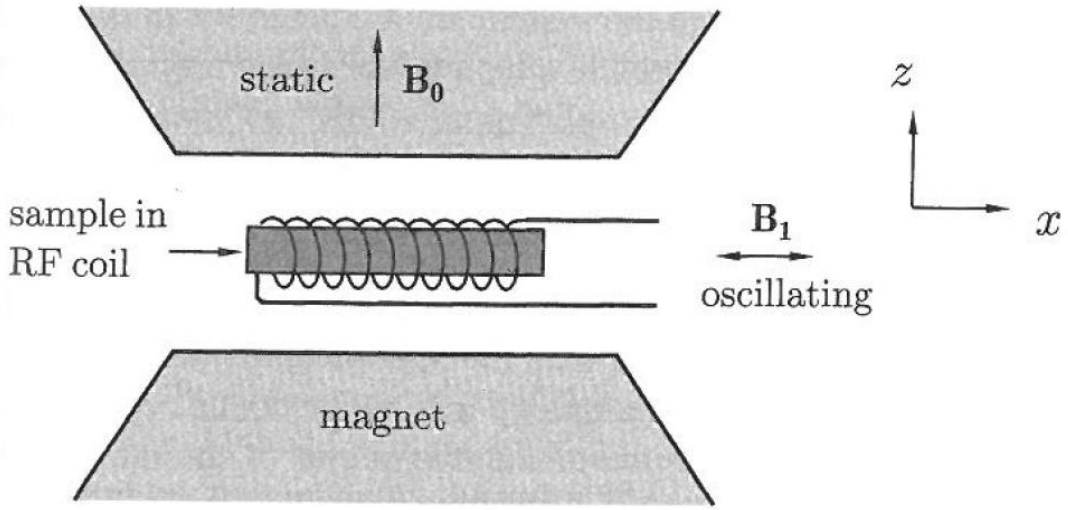

Fig. 3.9 Schematic diagram of an NMR experiment. The sample sits inside a radio frequency (RF) coil which produces an oscillating RF field. A highly homogenous static magnetic field is provided by a magnet. The static field $\mathbf{B}_0$ and the oscillating field $\mathbf{B}_1$ are perpendicular to each other. In a real experiment, the sample would be much smaller than is shown here so that it experiences a uniform field from the RF coil.

Zeeman splitting

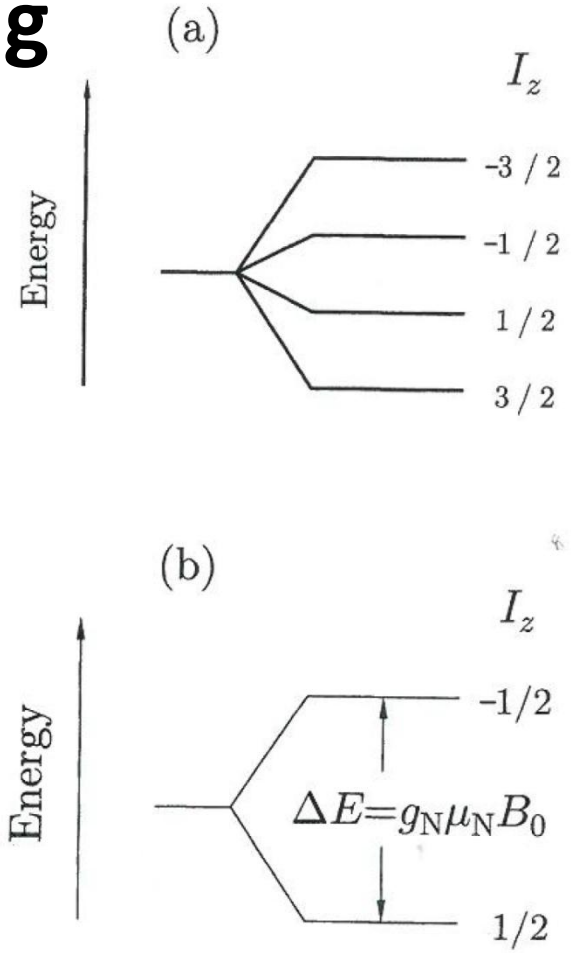

Fig. 3.10 (a) The four levels from an $I = \frac{3}{2}$ nucleus. (b) In the simpler case of an $I = \frac{1}{2}$ nucleus, there are just two levels. These two nuclear levels are separated by an energy $\Delta E = g_N \mu_N B_0$; the lower (upper) level corresponds to the nuclear magnetic moment lying parallel (antiparallel) to the magnetic field B_0.

ESR experiment

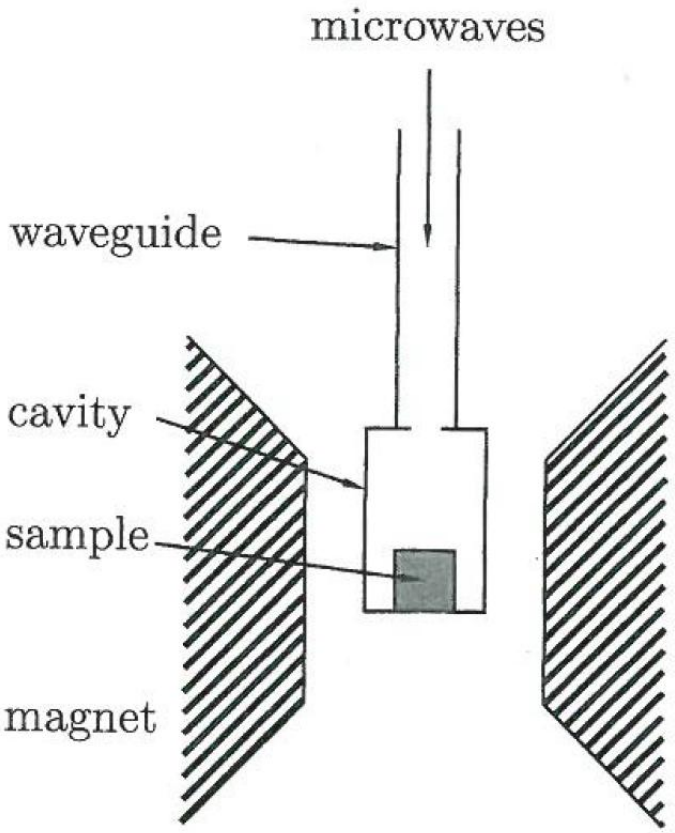

Fig. 3.14 Schematic diagram of an ESR experiment. Microwaves enter a cavity via a waveguide and the absorption of microwaves induced by a resonance is measured by monitoring the Q-factor of the cavity. The sample must be placed in the centre of the magnet, where the field is most clearly uniform.

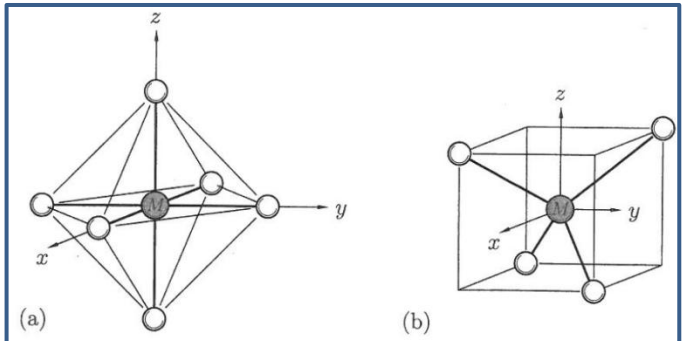

Fig. 3.2 A metal atom M in an (a) octahedral and (b) tetrahedral environment. The octahedral environment is found in many transition metal oxides where oxygen anions sit on the corners of an octahedron with the metal atom at the centre. The tetrahedral environment can be conveniently described by considering alternate corners of a cube as shown.

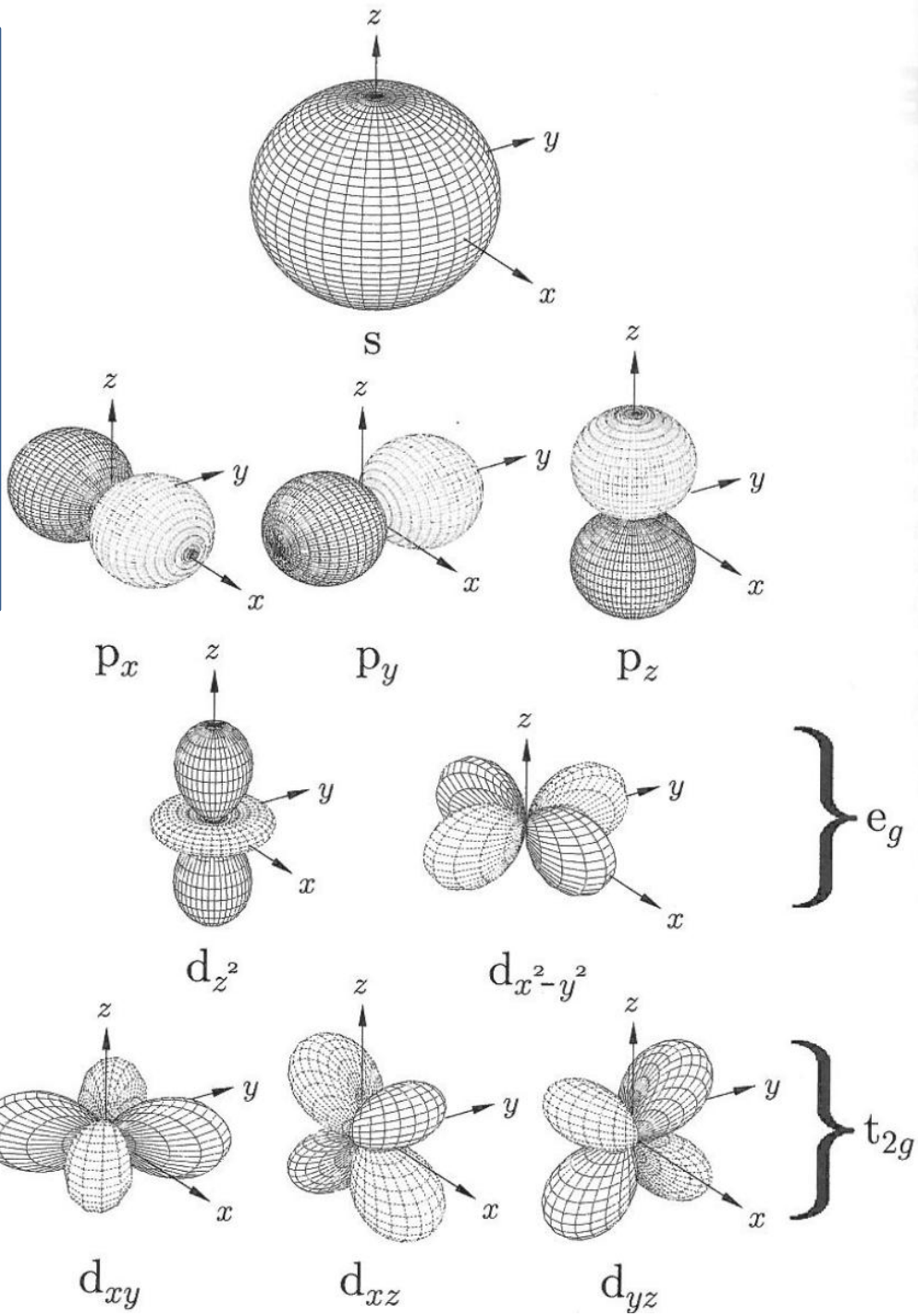

Fig. 3.1 The angular distribution of the s, p and d orbitals. The d_{z^2} and $d_{x^2-y^2}$ levels are grouped together and called the e_g levels. The d_{xy}, d_{xz} and d_{yz} levels are grouped together and called the t_{2g} levels. The d_{z^2} orbital is sometimes referred to as $d_{3z^2-r^2}$.

Crystal field splitting

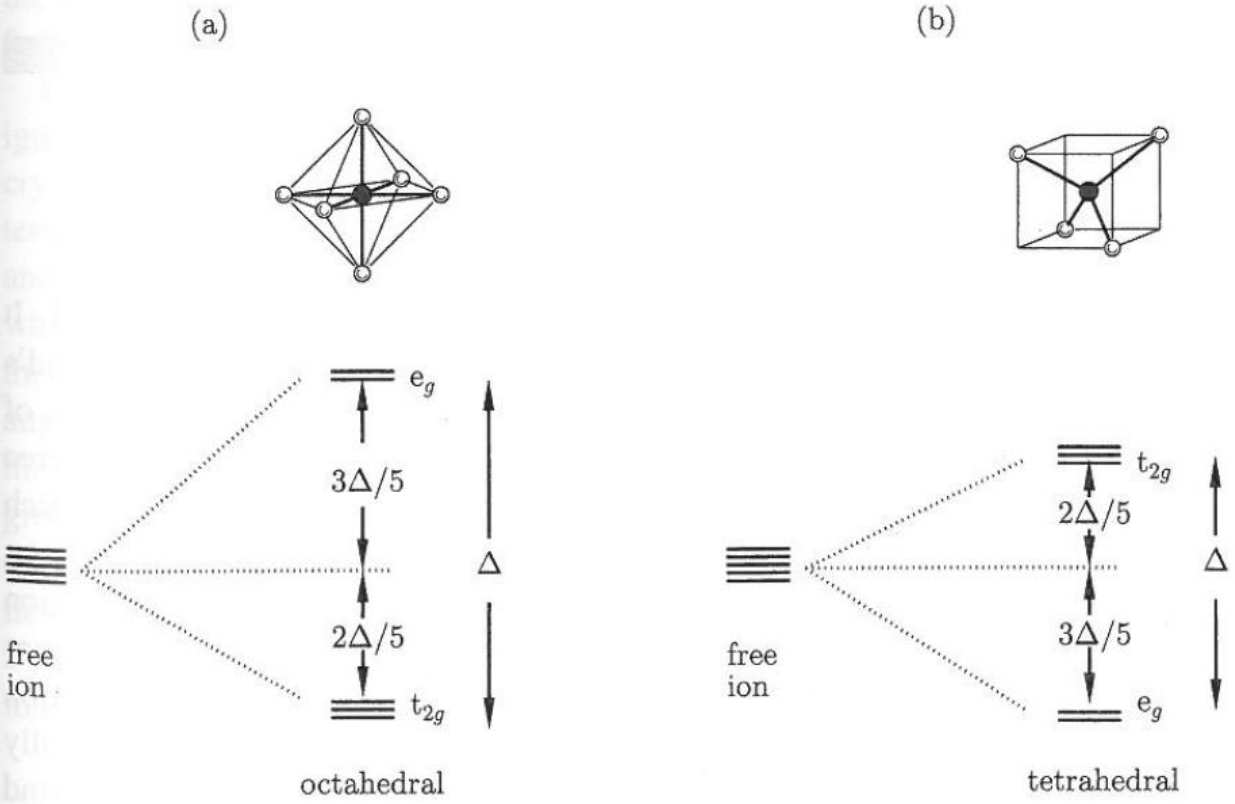

Fig. 3.4 The crystal field in an (a) octahedral and (b) tetrahedral environment.

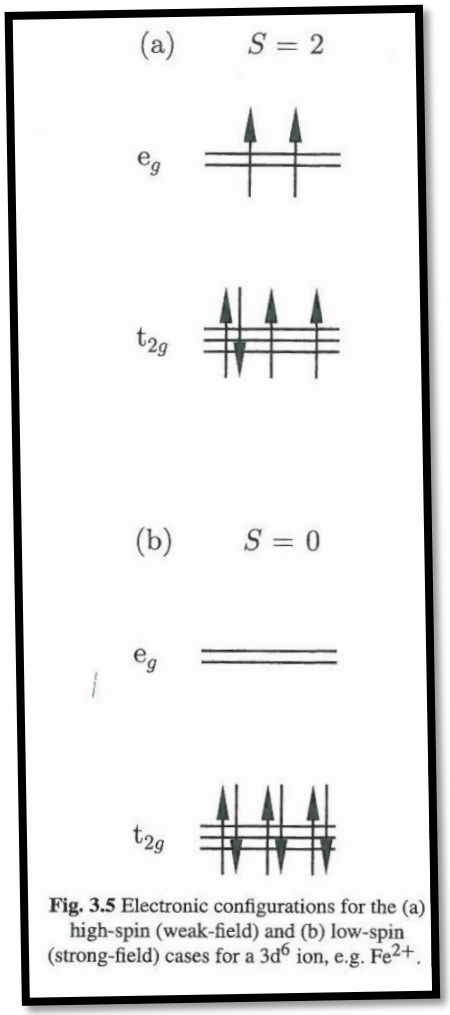

Fig. 3.5 Electronic configurations for the (a) high-spin (weak-field) and (b) low-spin (strong-field) cases for a $3d^6$ ion, e.g. Fe^{2+}.

ESR schematics

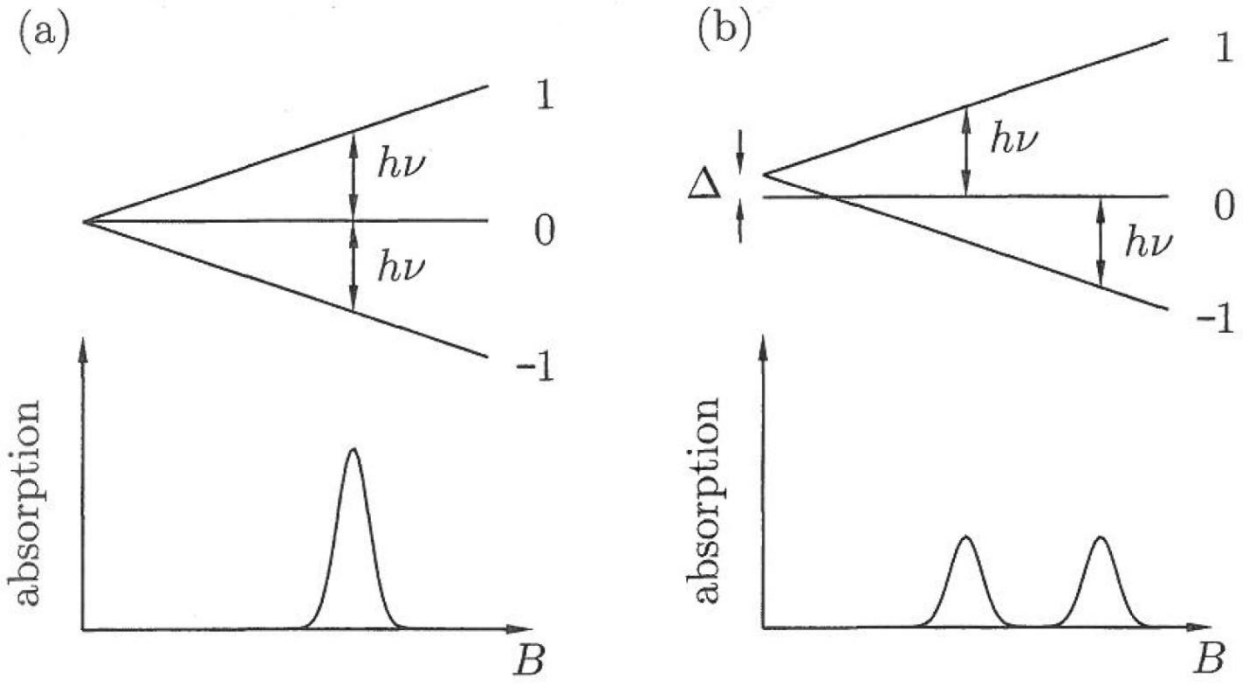

Fig. 3.15 ESR in an ion with $J = 1$ such as Ni^{2+} with (a) no crystal field splitting (leading to a single ESR line) and (b) crystal field splitting Δ (leading to two ESR lines).